

Ion-beam laser fluorescence measurement of Xe^+ hyperfine structure*

R. A. Holt, S. D. Rosner, and T. D. Gaily

Department of Physics, University of Western Ontario, London, Ontario N6A 3K7, Canada

(Received 23 February 1977)

Laser-induced fluorescence from a beam of xenon ions has been used to determine the hyperfine structures of two levels from the $5p^4 5d$ and $5p^4 6p$ excited configurations of $^{129}\text{Xe}^+$ and $^{131}\text{Xe}^+$. The coupling constants (in MHz) were found to be as follows: $A_{129}(6p^4 P_{5/2}^o) = -1667.5 \pm 18.7$, $A_{129}(5d^4 D_{7/2}) = -515.7 \pm 8.9$, $A_{131}(6p^4 P_{5/2}^o) = 487.5 \pm 5.2$, $B_{131}(6p^4 P_{5/2}^o) = -107.2 \pm 52.3$, $A_{131}(5d^4 D_{7/2}) = 149.4 \pm 3.2$, and $B_{131}(5d^4 D_{7/2}) = 76.1 \pm 27.5$. The data also yielded values for the very small isotope shifts.

I. INTRODUCTION

In recent years a great deal of theoretical and experimental effort has been devoted to understanding the inert-gas ions, in large part because of their importance to laser physics. Serious discrepancies remain, however, between theoretical and experimental values for such quantities as excited state lifetimes and oscillator strengths.¹ Particularly in the case of the heavier ions, such as Xe^+ , the presence of relativistic effects requires that a successful theoretical calculation employ sophisticated intermediate coupling multiconfiguration wave functions. Frequently these wave functions are determined from fine structure and atomic g -factor data; but, when it is available, hyperfine structure information can lend invaluable aid. In this paper we will present the results of a measurement of the hyperfine structures of the $5p^4 5d^4 D_{7/2}$ and $5p^4 6p^4 P_{5/2}^o$ levels² of Xe^+ by an ion beam laser-induced fluorescence method. The information about the $5p^4 5d$ configuration is particularly timely, as the existing level assignments have recently been questioned, and a reanalysis of this configuration is currently in progress.¹ The present experimental approach will be seen to be much cleaner and more accurate than the usual discharge tube techniques.

II. EXPERIMENTAL METHOD

Our method was to view the fluorescence induced at the intersection of a laser beam and a slow, nearly monoenergetic ion beam, as shown in Fig. 1. The Xe^+ beam was produced in a low-voltage dc arc source (Colutron Corp. Model 101), said by the manufacturer to have an energy spread $\Delta E \approx 0.1$ eV. The ions were accelerated to a final energy of 300 eV to 2 keV, collimated, and steered to the intersection region. Some of the ions emerge from the source in the metastable $5d^4 D_{7/2}$ level, and these can be excited to the $6p^4 P_{5/2}^o$ level by 605.12-nm photons (see Fig. 2).^{3,4} The lifetime of the upper level is about 10 nsec (Ref. 5); thus all

of the excited ions decay by spontaneous emission in the viewing region of the photomultiplier. A large fraction of the fluorescence is at 529.22 nm, so this region of the spectrum was isolated by an interference filter in front of the photomultiplier. To obtain a spectrum, the single-mode cw dye laser was scanned electronically while the photocurrent was recorded.

The mean angle of intersection of the laser and ion beams, θ_0 , was chosen to be $\approx 8^\circ$ in order to narrow the Doppler width of the absorption profiles. Because of the small ΔE of the ions, the resolution was limited principally by the variation of the Doppler shift with intersection angle ($\Delta\theta \approx 2^\circ$, mainly due to ion-beam divergence). This variation, which goes as $\cos\theta$, is quite rapid for $\theta_0 \approx 90^\circ$ and slow for small θ_0 . Earlier measurements³ at $\theta_0 = 90^\circ$, $E = 100$ eV had a resolution of ≈ 2.5 GHz, whereas the spectral line profiles observed in the present work had widths of ≈ 140 MHz.

The light source was a Spectra-Physics 580A tunable single-mode cw dye laser pumped by a Spectra-Physics 165 argon-ion laser. Smooth scans over large frequency ranges (≈ 9 GHz) at constant light intensity required a modification of the standard Spectra-Physics scanning system. Normally, the spacing of the laser's mode-selecting intracavity étalon is varied by applying a voltage ramp to its piezoelectric transducer (PZT),

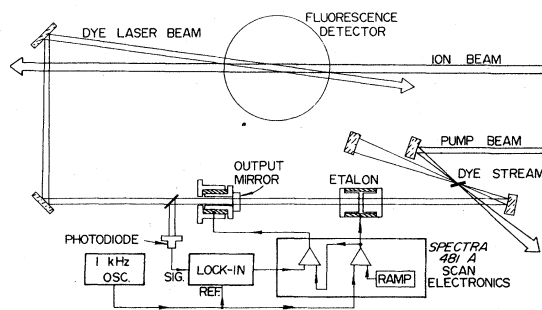
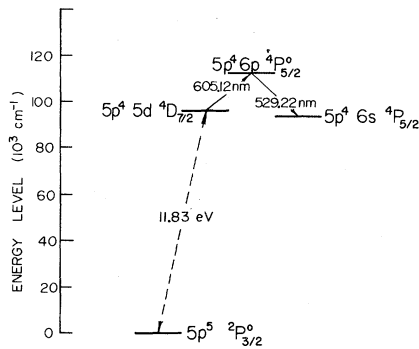


FIG. 1. Schematic diagram of the experimental apparatus.

FIG. 2. Partial Grotrian diagram of Xe^+ .

and the laser cavity is made to track the étalon by applying a similar but amplified ramp to the output mirror's PZT, with automatic resets of this voltage to keep it below the maximum allowable PZT voltage. Usually it is difficult to scan over large frequency intervals by this means without occasional mode hops and constant AM and FM jitter. To overcome this difficulty, we added active feedback stabilization to correct the output mirror's position continuously (see Fig. 1). The error signal for the loop was generated by modulating the étalon PZT at 1 kHz, thereby producing an amplitude modulation of the light output when the étalon and cavity transmission peaks did not coincide. A silicon photodiode viewing a portion of the laser light provided the input signal to a commercial lock-in amplifier. The output of the lock-in was fed into the summing junction of the cavity PZT drive circuit. The resulting frequency scan was extremely smooth, with no mode hops and reduced jitter. It was moderately linear, but for accurate measurements a series of frequency markers were required. These were obtained by monitoring the laser output with a temperature-stabilized confocal Fabry-Perot étalon of 1500-MHz free spectral range. The light transmitted through this reference cavity provided a signal to one channel of the dual pen chart recorder which was simultaneously recording the fluorescence photocurrent.

The photocurrent versus laser frequency curves obtained represent the combined spectra of all the isotopes of natural xenon. The components from one isotope are displaced from those of another by the isotope shift (predominantly the nuclear volume effect⁶ in this case) and by their relative Doppler shift. Because the Doppler shift could be varied at will, a very simple and direct method was available for the assignment of mass numbers to the observed spectral lines. An ion of mass M_i and energy E , with a transition in its rest frame at frequency $\nu_i(0)$, will absorb light

of frequency (in the lab frame)

$$\nu_i(E) = \nu_i(0)(1 + \beta_i \cos\theta_0)^{-1},$$

where

$$\beta_i = (2E/M_i c^2)^{1/2}.$$

Thus, if two masses differ by $\Delta M_{ij} = M_i - M_j$, their absorption frequencies will differ by

$$\begin{aligned} \nu_i(E) - \nu_j(E) \approx & \nu_i(0) - \nu_j(0) \\ & + \bar{\nu}_{ij} \cos\theta_0 (2E/\bar{M}_{ij} c^2)^{1/2} (\Delta M_{ij}/2\bar{M}_{ij}), \end{aligned}$$

in which $\bar{\nu}_{ij}$ is the average transition frequency of the two isotopes, and \bar{M}_{ij} is their average mass. This equation is correct to lowest order in ΔM_{ij} and $\nu_i(0) - \nu_j(0)$. If the observed frequency difference is plotted against $E^{1/2}$, a straight line whose slope is proportional to ΔM_{ij} will be obtained, making it quite easy to distinguish masses.

III. RESULTS

Fluorescence curves were taken at six energies in the 300-eV to 2-keV range. Examples at 300 eV, 700 eV, and 2 keV are shown in Figs. 3–5. As expected, groups of lines from a given isotope are seen to shift without changing their separation, and the lighter isotopes are shifted much farther toward lower frequency (to the right on the figures) than heavier isotopes. The intensities of the components are not those predicted by the usual formulas for weak light intensity because the laser is quite capable of saturating the stronger transitions. As

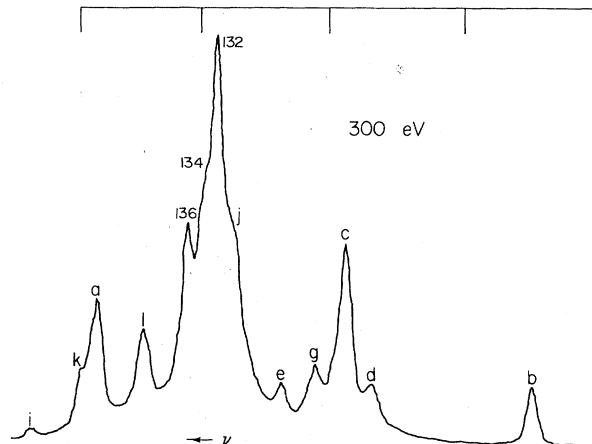


FIG. 3. Spectrum of fluorescence intensity vs laser wavelength at an ion beam energy of 300 eV. Scale at top indicates centers of calibration peaks; each division is 1500 MHz. Vertical scale is in arbitrary units. Lower case letters identify components from odd isotopes (see Table III). Lines from even isotopes are identified by mass number.

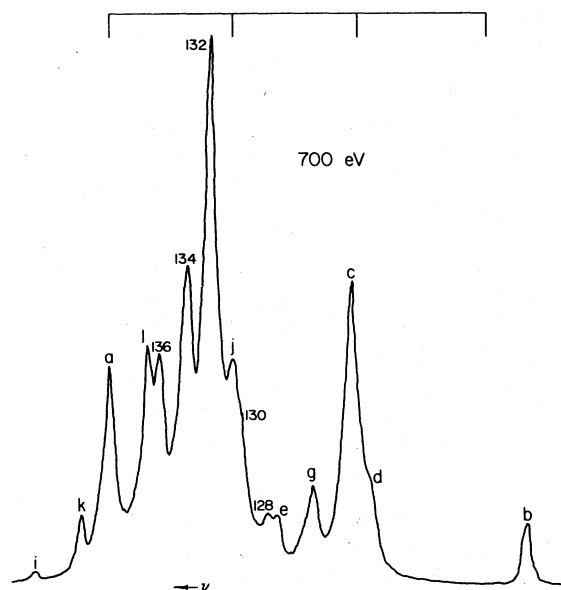


FIG. 4. Same as Fig. 3 for an ion energy of 700 eV.

a result, even the weakest components ($\Delta F = \Delta J + 2$) are clearly visible.

The locations of both the fluorescence peaks and the frequency calibration markers were digitized and recorded on punched cards with a Gerber GDDRS-3B digital data reduction system. The 1500-MHz marker locations were then fitted to a quadratic to yield a continuous frequency scale. The differential nonlinearity was typically $\pm 7\%$. Once the corrected frequencies of the fluorescence peaks were computed, Doppler shift analysis as discussed above yielded a mass number for each

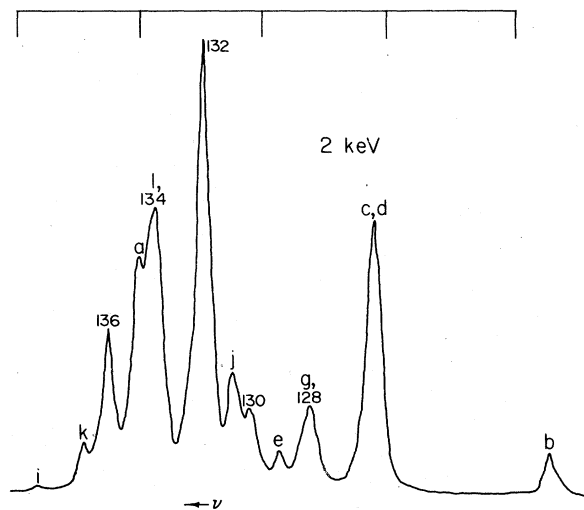


FIG. 5. Same as Fig. 3 for an ion energy of 2 keV.

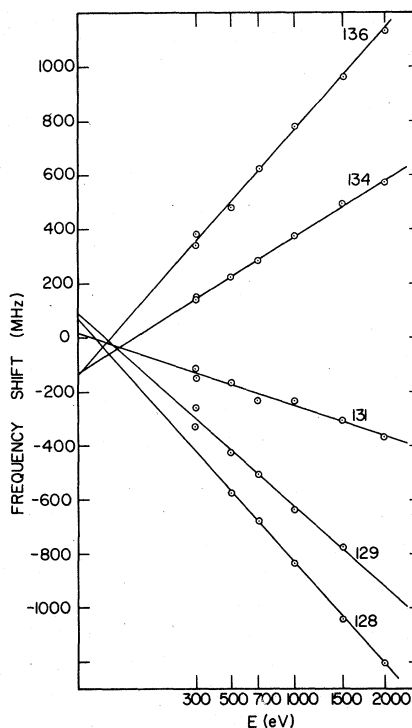


FIG. 6. Shift of spectral lines (relative to mass 132 line) vs ion beam energy. Horizontal axis is scaled as $E^{1/2}$. Lines for masses 129 and 131 were calculated from observed hyperfine structure.

peak. Figure 6 shows the straight-line least-squares fits for a number of frequency intervals versus $E^{1/2}$. In all cases the reference frequency is the mass 132 peak. (The odd isotopes' locations were determined from the hyperfine structure analysis which follows.) The zero-energy intercepts give the isotope shifts directly; the results are summarized in Table I. These shifts are very small, as would be expected for a transition in which the number of *s* electrons does not change,⁶ and it is quite remarkable that they can be observed at all. The very small separation be-

TABLE I. Isotope shifts in the 605.1-nm transition of Xe⁺.

| Mass | Frequency shift (MHz) ^a |
|------|------------------------------------|
| 128 | 66 ± 20 ^b |
| 129 | 91 ± 20 |
| 131 | 15 ± 20 |
| 134 | -130 ± 20 |
| 136 | -135 ± 20 |

^aRelative to mass 132.

^bError estimates based upon systematic errors in locating peak positions.

TABLE II. Hyperfine coupling constants^a in Xe⁺.

| Run No. | Ion energy (eV) | ¹²⁹ Xe ⁺ | | ¹³¹ Xe ⁺ | | | |
|---------|-----------------|--------------------------------|------------------------|--------------------------------|-------------------------|------------------------|------------------------|
| | | A' ₁₂₉ (MHz) | A ₁₂₉ (MHz) | A' ₁₃₁ (MHz) | B' ₁₃₁ (MHz) | A ₁₃₁ (MHz) | B ₁₃₁ (MHz) |
| 1 | 300 | -1691.3 | -527.3 | 490.3 | -24.1 | 150.5 | 90.2 |
| 2 | 300 | -1680.7 | -524.5 | 491.8 | -101.7 | 149.2 | 58.3 |
| 3 | 500 | -1680.0 | -518.3 | 484.8 | -59.2 | 145.9 | 111.8 |
| 4 | 700 | -1652.0 | -508.0 | 495.5 | -164.9 | 154.0 | 50.2 |
| 5 | 1000 | -1653.7 | -507.0 | 486.0 | -106.4 | 147.4 | 43.5 |
| 6 | 1500 | -1647.0 | -509.3 | 481.5 | -128.9 | 146.0 | 71.4 |
| 7 | 2000 | | | 482.5 | -165.2 | 152.9 | 107.5 |
| Average | | -1667.5 | -515.7 | 487.5 | -107.2 | 149.4 | 76.1 |
| Error | | 18.7 | 8.9 | 5.2 | 52.3 | 3.2 | 27.5 |

^aPrimed and unprimed constants refer to the $6p^4P_{5/2}^o$ and $5d^4D_{7/2}$ levels, respectively.

tween masses 134 and 136 may be the result of attaining the neutron magic number 82 at mass 136.

The analysis of hyperfine structure is accomplished without any reference to Doppler shift information beyond the initial assignment of mass numbers. In the case of ¹²⁹Xe⁺ the nuclear spin is $\frac{1}{2}$, so there is only magnetic dipole hfs and hence only two coupling constants to fit, $A_{129}(5p^45d^4D_{7/2})$ and $A_{129}(5p^46p^4P_{5/2}^o)$, which will be referred to for the sake of brevity as A_{129} and A'_{129} , respectively. The ¹³¹Xe⁺ nucleus has $I = \frac{3}{2}$, and thus in addition to A_{131} and A'_{131} there are also electric quadrupole coupling constants B_{131} and B'_{131} to determine. Formulas for the hfs splittings are presented in the Appendix. The analysis of each fluorescence curve requires at least four frequency intervals to fit the ¹³¹Xe⁺ constants and two for ¹²⁹Xe⁺; in some cases more were available. A separate least-squares fit was used for each odd isotope in each spectrum. The results are summarized in Table II, and the computed hyperfine structures are displayed in Fig. 7. To include the effects of systematic errors from partial overlapping of peaks, the error estimates shown in Table II were chosen conservatively. One sample standard deviation

is quoted rather than the standard deviation of the mean. At present there are no theoretical predictions with which to compare the measured coupling constants. It is hoped that this experiment will lend impetus to theoretical work on this atomic system.

The ratios of the hyperfine constants can be used to compute the magnetic hyperfine anomaly for each atomic level.^{7,8} With the precision of the present experiment, these values are not very well determined; however, relatively modest improvements should bring them within our reach.

TABLE III. Hyperfine contributions to the 605.1-nm Xe⁺ transition.

| Component | F' ^a | F | ¹²⁹ Xe ⁺ |
|-----------|-----------------|---|---|
| | | | $\Delta\nu$ hfs |
| a | 2 | 3 | $-\frac{7}{4}A'_{129} + \frac{9}{4}A_{129}$ |
| b | 3 | 3 | $\frac{5}{4}A'_{129} + \frac{9}{4}A_{129}$ |
| c | 3 | 4 | $\frac{5}{4}A'_{129} - \frac{7}{4}A_{129}$ |
| Component | F' | F | ¹³¹ Xe ⁺ |
| | | | $\Delta\nu$ hfs |
| d | 1 | 2 | $-\frac{21}{4}A'_{131} + \frac{27}{4}A_{131} + \frac{7}{10}B'_{131} - \frac{15}{28}B_{131}$ |
| e | 2 | 2 | $-\frac{13}{4}A'_{131} + \frac{27}{4}A_{131} - \frac{1}{10}B'_{131} - \frac{15}{28}B_{131}$ |
| f | 3 | 2 | $-\frac{1}{4}A'_{131} + \frac{27}{4}A_{131} - \frac{11}{20}B'_{131} - \frac{15}{28}B_{131}$ |
| g | 2 | 3 | $-\frac{13}{4}A'_{131} + \frac{15}{4}A_{131} - \frac{1}{10}B'_{131} + \frac{5}{28}B_{131}$ |
| h | 3 | 3 | $-\frac{1}{4}A'_{131} + \frac{15}{4}A_{131} - \frac{11}{20}B'_{131} + \frac{5}{28}B_{131}$ |
| i | 4 | 3 | $\frac{15}{4}A'_{131} + \frac{15}{4}A_{131} + \frac{1}{4}B'_{131} + \frac{5}{28}B_{131}$ |
| j | 3 | 4 | $-\frac{1}{4}A'_{131} - \frac{1}{4}A_{131} - \frac{11}{20}B'_{131} + \frac{13}{28}B_{131}$ |
| k | 4 | 4 | $\frac{15}{4}A'_{131} - \frac{1}{4}A_{131} + \frac{1}{4}B'_{131} + \frac{13}{28}B_{131}$ |
| l | 4 | 5 | $\frac{15}{4}A'_{131} - \frac{21}{4}A_{131} + \frac{1}{4}B'_{131} - \frac{1}{4}B_{131}$ |

^aF' and F refer to the total angular momenta of the $6p^4P_{5/2}^o$ and $5d^4D_{7/2}$ levels, respectively.

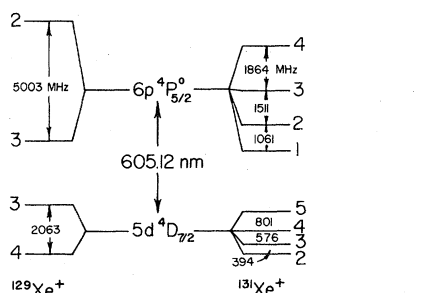


FIG. 7. Hyperfine structures of the $5d^4D_{7/2}$ and $6p^4P_{5/2}^o$ levels of Xe⁺ based upon constants in Table II. Hyperfine levels are labeled by their F values.

IV. CONCLUSIONS

A precise measurement of the hyperfine structures of two excited levels of Xe⁺ has been carried out by laser-induced fluorescence spectroscopy on an ion beam. The method clearly yields much better resolution than discharge tube techniques.⁴ With the planned addition of a mass spectrometer it will be possible to investigate the spectra of numerous ionized molecules and atoms without any doubt as to the species under study. (This is often a problem in discharge tube experiments. In the present case the simplicity of the optical spectrum allowed us to avoid mass separation.) Furthermore, in the near future we expect to present results of a radiofrequency investigation of Xe⁺ hyperfine structure by a method we have recently applied to Na₂ molecules.⁹ This will increase the resolution by three orders of magnitude and the accuracy by an even greater factor.

ACKNOWLEDGMENTS

We wish to thank I. Schmidt for valuable technical assistance.

APPENDIX

The hyperfine interaction between a nucleus of spin I and electrons in a state of total angular momentum J has the expectation value¹⁰

$$W_F = \frac{1}{2}AC + \frac{1}{4}B \frac{\frac{3}{2}C(C+1) - 2I(I+1)J(J+1)}{I(2I-1)J(2J-1)},$$

in which F is the total angular momentum of the system and

$$C = F(F+1) - I(I+1) - J(J+1).$$

The hyperfine contributions to the optical transition frequencies are expressed in terms of the hyperfine coupling constants in Table III.

*Work supported in part by the National Research Council of Canada and by the University of Western Ontario.

¹S. Garpman and N. Spector, *J. Opt. Soc. Am.* **66**, 904 (1976).

²Use of Russell-Saunders notation is only for purposes of identification and does not imply that L - S coupling is an accurate description of these levels.

³S. D. Rosner, T. D. Gaily, and R. A. Holt, *J. Phys. B.* **9**, L489 (1976).

⁴M. Elbel, C. Höhle, H. Hühnermann, Th. Meier, and B. Vettin, *Opt. Commun.* **19**, 412 (1976).

⁵E. Jiménez, J. Campos, and C. Sánchez del Rfo, *J. Opt. Soc. Am.* **64**, 1009 (1974).

⁶D. N. Stacey, *Rep. Prog. Phys.* **29**, 171 (1966).

⁷J. Eisinger and V. Jaccarino, *Rev. Mod. Phys.* **30**, 528 (1958).

⁸H. H. Stroke, R. J. Blin-Stoyle, and V. Jaccarino, *Phys. Rev.* **123**, 1326 (1961).

⁹S. D. Rosner, R. A. Holt, and T. D. Gaily, *Phys. Rev. Lett.* **35**, 785 (1975).

¹⁰H. G. Kuhn, *Atomic Spectra*, 2nd ed. (Longmans, London, 1969), p. 351.